Chapter 4 ^{3}He Polarimetry

4.1 NMR-AFP Polarimetry

Knowledge of the ^{3}He polarization is critical for measuring the extended GDH sum rule. The polarization is monitored throughout the experiment by the Nuclear Magnetic Resonance (NMR) technique of Adiabatic Fast Passage (AFP) [63]. The strength of the NMR signal is proportional to the amount of polarization.

Classically, NMR-AFP is described by considering one free particle with spin $\mathbf{I}$ and magnetic moment $\mathbf{M} = \gamma \mathbf{I}$, where γ is the gyromagnetic ratio. When this particle is placed in a magnetic field $\mathbf{H}$, its moment experiences a torque:

$$\frac{d\mathbf{M}}{dt} = \gamma \mathbf{M} \wedge \mathbf{H}. \tag{4.1}$$

It's useful to transform this equation into a frame that is rotating at a frequency and direction given by $-\boldsymbol{\omega}$. Following [64], Eq. 4.1 becomes

$$\frac{\partial \mathbf{M}}{\partial t} = \gamma \mathbf{M} \wedge \left(\mathbf{H} - \frac{\boldsymbol{\omega}}{\gamma} \right). \tag{4.2}$$

The magnetic field $\mathbf{H}$ in Eq. 4.1 is now replaced by an effective field comprised of the laboratory field and a fictitious field, $\mathbf{H}_e = \left(\mathbf{H} - \frac{\boldsymbol{\omega}}{\gamma} \right)$.

In our case, the laboratory field is a holding field in the z-direction, $H_z \hat{\mathbf{k}}$, and a RF field in the x-direction, $\mathbf{H}_{rf} = 2H_1 \cos(\omega_0 t) \hat{\mathbf{i}}$. The RF field can be expressed in terms of two counter-rotating components:

$$\mathbf{H}_{rf} = H_1 \hat{\mathbf{i}}'_+ + H_1 \hat{\mathbf{i}}'_-, \tag{4.3}$$

where $\hat{\mathbf{i}}'_{\pm} = \cos(\omega_0 t)\hat{\mathbf{i}} \pm \sin(\omega_0 t)\hat{\mathbf{j}}$. If we set $\boldsymbol{\omega}$ equal to $\omega_0\hat{\mathbf{k}}$, then the effective field in the rotating system becomes

$$\mathbf{H}_e = \left(H_z - \frac{\omega_0}{\gamma}\right)\hat{\mathbf{k}} + H_1\hat{\mathbf{i}}'. \tag{4.4}$$

The ^{3}He average magnetic moment, $< \mathbf{M} >$, aligns itself with the effective field.

During AFP, the holding field changes in value such that it passes through the value $|\frac{\omega_o}{\gamma}|$. The angle that $< \mathbf{M} >$ makes with the z-axis increases until $H_z = \frac{\omega_0}{\gamma}$ and the spins are at an angle of 90° (Figure 4.1). For our conditions $\omega_0 = 2\pi f$, where f=91 kHz, and γ for ^{3}He is $-20378 s^{-1}G^{-1}$ making $|\frac{\omega_0}{\gamma}| = 28.06G$. When this resonance condition is met, the ^{3}He average magnetic moment induces an EMF signal in the pickup coils located on both sides of the target chamber. As the holding field increases in value beyond $|\frac{\omega_o}{\gamma}|$, the spins end up pointing in the opposite direction. This process is called a spin flip.

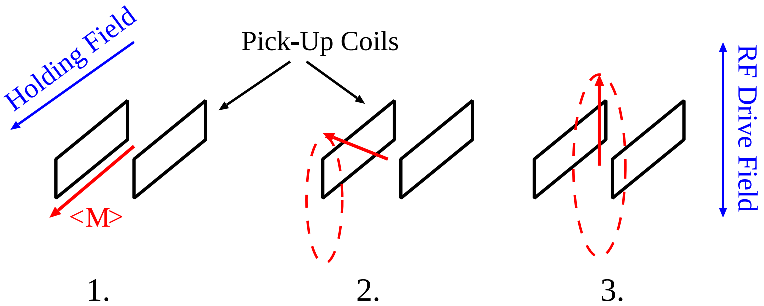

Figure 4.1: The process of an AFP-NMR spin flip. 1) Initially the spins are aligned with the holding field. 2) A 91 kHz RF field is applied, and the magnetic moment of the ^{3}He begins to precess about the z axis as the holding field moves towards 28.06 G. 3) When the holding field is at 28.06 G the ^{3}He spins are rotating perpendicular to the z-axis, an EMF signal is induced in the pickup coils.

Measurements of the ^{3}He polarization was done by scanning the holding field from 25 to 32 G and back, at a rate of 1.2 G/s. This procedure results in two spin flips, inducing an EMF signal twice. The signal size is proportional to the transverse component of the magnetization:

$$S_{He}^{nmr}(t) \propto \frac{< \mathbf{M} > H_1}{\sqrt{(H_z(t) + \frac{\omega_0}{\gamma})^2 + H_1^2}}, \tag{4.5}$$

where

$$< \mathbf{M} >= P_{He}\mu_{He}[^3\mathrm{He}]. \tag{4.6}$$

An example of a NMR signal can be seen in Figure 4.2. Signals were fitted to Eq. 4.5, plus a slope and constant: $m \cdot H_z(t) + C$. It is the fitted amplitude that is considered to be proportional to the polarization.

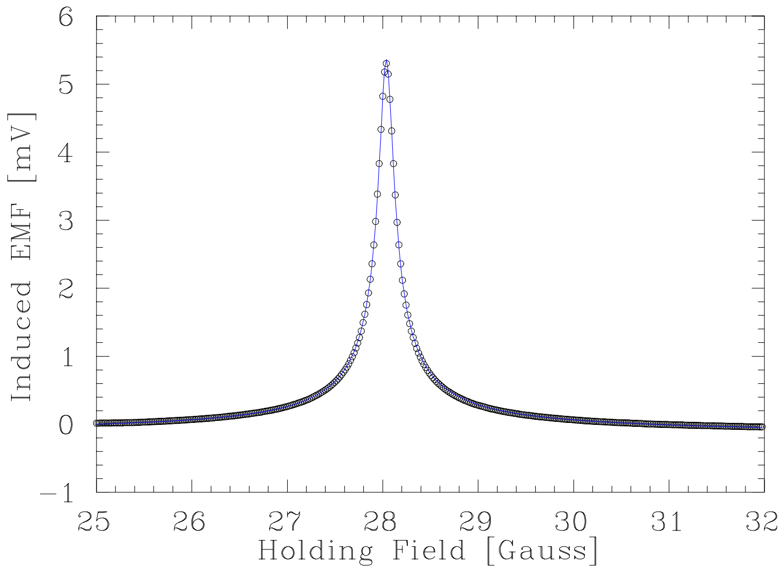

Figure 4.2: A NMR signal.

The condition for adiabatic fast passage is met when:

$$\frac{D|\nabla H_z|^2}{H_1^2} \ll \frac{\dot{H}_z}{H_1} \ll \omega_0, \tag{4.7}$$

where D is the ^{3}He diffusion rate. The holding field rate of change must be slow enough that the spins can follow adiabatically and fast enough that spin relaxation at resonance is minimal. For our conditions, both considerations were easily met:

$$\frac{D|\nabla H_z|^2}{H_1^2} \approx 10^{-2}[s^{-1}] \ll \frac{\dot{H}_z}{H_1} = 24[s^{-1}] \ll \omega_0 = 9.1 \times 10^4[s^{-1}]. \tag{4.8}$$

4.2 Calibration

In order to extract a polarization value for the ^{3}He, the NMR system needed to be calibrated. This was done by placing a substance with a known polarization between the pickup coils, taking a NMR measurement, and calculating a constant of proportionality, κ, between signal height and polarization. This constant can then be used to extract the polarization of ^{3}He:

$$S_{He} = \kappa P_{He}. \tag{4.9}$$

The constant of proportionality depends on several factors. Some of the factors (e.g., position and density) depend on which target cell is being used. The other factors are independent of the target cell and measure the NMR system's responsiveness, or amount of signal seen for a given spin. Therefore, the calibration constant κ for each cell is a product of two parts:

$$\kappa_{cell} = \kappa^* \underbrace{\Phi_{He} G^Q_{He} n_o \left(\frac{n_c}{n_o}\right)}_{\text{cell dependent}}, \tag{4.10}$$

where κ^* is the responsiveness of the system, Φ_{He} is the geometrical flux produced by a particular cell, and G^Q_{He} is a measure of the LRC circuit's gain at the time of the measurement. The purpose of calibration is to determine κ^*.

Two methods were used to calibrate the NMR system. The first method relied on the thermally polarized protons contained in water. Their polarization is given by the Boltzmann distribution:

$$P_w^{th} = \tanh \frac{\mu_p B}{kT} \approx 7 \times 10^{-9}, \tag{4.11}$$

where μ_p is the magnetic moment of the proton, B is the magnetic field, k is Boltzmann's constant, and T is the temperature. The second method used the polarization of ^{3}He as determined by the electron paramagnetic resonance signal coming from polarized Rb [65].

4.2.1 The Calibration Constant κ_w^*

For the water calibration, a water cell with the same geometry as a helium cell was filled with de-oxygenated, de-ionized water. This cell was mounted in the same setup as the helium cells, and a NMR measurement was taken. The thermal polarization of the protons in the water at room temperature and at the field strength used during the experiment is quite low (Eq. 4.11). Typically 100 to 300 NMR sweeps were taken and averaged. Once a water signal was obtained, a fit was performed to determine the amplitude: S_w. With the water signal, the calculated thermal polarization, and a number of other factors, the calibration factor κ_w^* can be found. The calibration becomes:

$$\kappa_w^* = \frac{S_w}{P_w^{th}} \cdot \frac{\mu_{He}}{\mu_p} \cdot \frac{G_{He}^{pre}}{G_w^{pre}} \cdot \frac{1}{G_w^Q} \cdot \frac{1}{\Phi_w} \cdot \frac{1}{n_p} \cdot C_{\frac{\delta H}{H}} \cdot C_{cover}, \tag{4.12}$$

where $G_{He,w}^{pre}$ are the settings for the preamplifier, n_p is the number density of the protons (2482 amg.), and $C_{\frac{\delta H}{H}}$ and C_{cover} are slight correction factors to the water signal. Details of these various parameters for κ_w^* are discussed below.

4.2.2 Water Signal and Thermal Polarization

There are two challenging aspects of using water as a calibration medium. One is that the thermal polarization present depends on the holding field strength, which changes between 18 and 25 Gauss. The other complication is that the proton spins in water tend to relax away from the direction of the effective field, H_{eff}, towards the direction of the holding field, H_z. This relaxation process can be described by [63]

$$\frac{dM_z}{dt} = -(M_z - <\mathbf{M}>)/T_1, \tag{4.13}$$

where M_z is the component of the average magnetic moment,$<\mathbf{M}>$, in the z-direction and T_1 is the longitudinal relaxation time. For protons in water, T_1 is on the order of a couple of seconds. The proton polarization increases as the field changes from 18 to 25 Gauss and loses polarization as the angle between H_{eff} and H_z increases. By the time the field reaches 25 Gauss, all of the spins have relaxed back toward the holding field direction. This does not occur for ^{3}He because the relaxation time is on the order of 10^5 seconds. As the field sweeps back down from 25 to 18 Gauss, the spins will again go through resonance but this time starting with a higher polarization.

In order to understand the amount of thermal polarization at the moment that the spins are at resonance, we use the Bloch equations. These equations describe the three components of the polarization in the rotating reference frame: x', y', and z':

$$\begin{aligned}
\frac{dP_{x'}}{dt} &= \gamma P_{y'}(H_z(t) - \frac{\omega}{\gamma}) - \frac{P_{x'} - \chi H_1}{T_2}, && (4.14)\\
\frac{dP_{y'}}{dt} &= -\gamma P_{x'}(H_z(t) - \frac{\omega}{\gamma}) + \gamma P_{z'} H_1 - \frac{P_{y'}}{T_2}, && (4.15)\\
\frac{dP_{z'}}{dt} &= -\gamma P_{y'} H_1 - \frac{P_{z'} - \chi H_z(t)}{T_1}, && (4.16)\\
H_z(t) &= \frac{\omega}{\gamma} + \alpha t, && (4.17)
\end{aligned}$$

where α is the sweep rate of the holding field (1.2 G s^{-1}), T_2 is the transverse relaxation time, H_1 is the value of the RF field (90.8$\pm$0.5 mG), ω is the radial frequency of the RF field ($2\pi f$, f=91kHz), χ is the magnetic susceptibility ($3.4616\pm0.0117\times10^{-10}$ G^{-1} at 22°), and γ is the gyromagnetic ratio of the proton (2.6752×10^4 s^{-1} G^{-1}).

The Bloch equations do not have an analytic solution. However, the equations can be solved numerically in order to determine the shape and behavior of the resonance signal under different conditions. It was found that T_2 did not significantly effect the shape of the signal but did effect the height. If, for the purpose of creating an analytic solution, we set $T_1 = T_2$ and assume that under adiabatic conditions the polarization follows the effective field ($H_{eff} = (H(t) - \omega/\gamma)\hat{k} + H_1\hat{i}$) in the rotating coordinate system, then the Bloch equations can be reduced to one equation for $P_{eff} = \sqrt{P_x^2 + P_y^2 + P_z^2}$:

$$\frac{dP_{eff}}{dt} = \frac{1}{T_1}(P_{eq}(t) - P_{eff}) \tag{4.18}$$

where

$$P_{eq} = \chi \left(\frac{H(t)(H(t) - \frac{\omega}{\gamma}) + H_1^2}{\sqrt{H_1^2 + (H(t) - \frac{\omega}{\gamma})^2}} \right). \tag{4.19}$$

The integral solution is given by:

$$P(t) = e^{-(t-t_0)/T_1} \left(P(t_0) + \frac{1}{T_1} \int_{t_0}^{t} e^{(t'-t_0)/T_1} P_{eq}(t')dt' \right). \tag{4.20}$$

By expanding the exponential and the denominator of P_{eq} to first order in t', the integral can be solved. This will yield an approximate analytic solution to the Bloch equations. Comparison of the approximate solution to the integral solution showed agreement within 0.4% of the peak height everywhere along the curve. The analytic solution allows one to fit the water signal in order to determine the signal height. The thermal polarization detected at any time is given by P_x; therefore, P_{th} is just equal to the maximum value of P_x.

Three water signals were taken during the experiment. They were conducted on the following dates: Sept. 25th, Nov. 3rd, and Nov. 25th. The experiment collected data from Sept. 26th to Dec. 24th, 1998.

Figure 4.3 shows the water signal taken on Sept. 25th. The *UP* and *DOWN* sweeps are each comprised of 373 points, each one of which represents the EMF pickup from the coils at that particular holding field value. The uncertainty assigned to each point comes from the standard deviation of the values recorded for that particular field. Also, shown in Figure 4.3 are the fits to the *UP* and *DOWN* sweeps. The fitting function is the analytical solution to the Bloch equations where $T_1 = T_2 = 2.95$ s [66]. The uncertainty in the fitted amplitude is taken to be less than 2%.

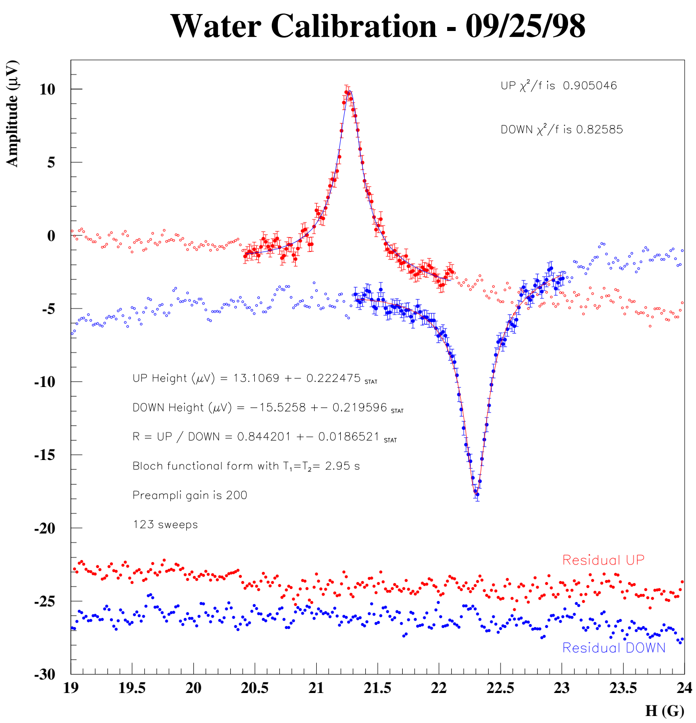

Figure 4.3: The fit to the *UP* and *DOWN* sweeps for the water signal taken on 9/25/98. The position of the resonance for the *DOWN* sweep has been shifted in this plot.

To find a value of T_1 for de-oxygenated, de-ionized water, the ratio of the *UP* and *DOWN* sweep amplitudes was studied. Their ratio, $R = S_w^{UP} / S_w^{DOWN}$, has a strong T_1 dependence. An initial T_1 was chosen, the *UP* and *DOWN* water signals were fitted, the ratio calculated, and a new T_1 was predicted. This new T_1 was then plugged into the analytic solution and the *UP* and *DOWN* signals were re-fitted predicting T_1 again.

The process is repeated until the predicted T_1 matches the initial T_1 used. By taking the weighted average of the ratio from the three water signals, it was found that

$$R = 0.839 \pm 0.010, \tag{4.21}$$

which leads to a value for T_1 of

$$T_1 = 3.0 \pm 0.4s. \tag{4.22}$$

This value is in good agreement with the world value for de-oxygenated water of $T_1 = 2.95s$ [66] at $20°C$. The value of T_2 is related to the value of T_1 [67]: $\frac{1}{T_1} - \frac{1}{T_2} = 0.125s^{-1}$. If we assume that T_1 and T_2 are 100% correlated, and for a RF field, H_1, of 90.8 ± 0.5 mG, then

$$T_2 = 2.7 \pm 0.4s. \tag{4.23}$$

The analytical equation that is used to determine S_w assumes that $T_1 = T_2$. The fact that T_1 does not equal T_2 causes the fitted amplitude to be decreased by a small amount. By solving the Bloch equations numerically and comparing to the case when $T_1 = T_2$, it was determined that the *UP* and *DOWN* thermal polarizations needed to be corrected up by 0.36% and 0.21% respectively with negligible uncertainty.

The calculated thermal polarizations at the moment when resonance occurs is

$$P^{th}_{UP} = 6.415 \times 10^{-9} \qquad \text{and} \qquad P^{th}_{DOWN} = 7.655 \times 10^{-9}. \tag{4.24}$$

The total uncertainty (Table 4.2.2) on these polarizations comes mainly from the uncertainty in the initial and maximum value of the holding field during a sweep.

The fitted amplitudes to the three water calibrations are listed in Table 4.2. For the purposes of calculating κ_w, the fitted amplitudes for *UP* and *DOWN* sweeps will be divided by their corresponding thermal polarizations and then averaged, yielding just one value of S_w/P^{th}_w for each water calibration. This value, divided by the gain

Parameter	T_1	Initial Field	Integration	Temperature	Total
Value	3.0 ± 0.4 s	$18(25) \pm 0.5$ G		22 ± 1°C	
Uncertainty	0.3%	1.1%	0.5%	0.3%	1.3%

Table 4.1: Systematic uncertainties on P_w^{th}.

of the preamplifier, is listed as *ave* in Table 4.2.

sweep direction	Date of water calibration		
	9/25/98	11/3/98	11/25/98
UP (μV)	13.11±0.22	6.48±0.12	66.85±0.89
DOWN (μV)	15.52±0.22	7.83±0.13	79.54±0.93
R	0.845 ± 0.019	0.828 ± 0.021	0.840 ± 0.015
G_w^{pre}	200	100	1000
# of sweeps	123	271	213
ave [mV/%]	101.9±1.1	102.1±1.3	104.5±0.9

Table 4.2: Fitted values for S_w with systematic uncertainties (μV) and the average of S_w/P_w^{th} for each water calibration divided by G_w^{pre}.

4.2.3 Corrections to the Water Signal

By comparing the resonance position of groups of 50 water sweeps, it was found that the initial and maximum holding field values drift at a rate of $\delta H/H = 0.001 hr^{-1}$. Because the computer assumes that the sweep always starts and stops at the same value, the signal is slightly broadened, and the peak height is reduced. In order to model this effect, a number of Lorentzian lines shapes were generated with their resonance positions shifted by an amount corresponding to the field drift. The Lorentzian line shapes were averaged and then fitted. The fitted height estimates the reduction in the amplitude due to the field drift. The amount of the correction necessary for each water signal is listed in Table 4.3. The assigned systematic uncertainty in the correction is taken to be $\pm 0.2\%$.

During the experiment, the RF Helmholtz coils were surrounded by an aluminum

Date	9/25/98	11/3/98	11/25/98
# of sweeps	123	271	213
$C_{\frac{\delta H}{H}}$	1.0035	1.0156	1.0099

Table 4.3: Values for $C_{\frac{\delta H}{H}}$.

sheet. This cover was not in place when a water signal was measured. Two tests were conducted with different target cells and at different polarization values. In both cases the lasers were turned off. Table 4.4 lists the NMR values and time recorded during each test, as well as the apparent rate of depolarization and the effect of the cover being off. Both tests found that the effect of the cover off was to increase the signal by 1.7%. To correct the water signal $C_{cover} = 0.983$. By assuming different loss mechanisms and seeing the effect on C_{cover}, a systematic uncertainty of 0.3% was determined.

Cell: *Blue*			Cell: *Jin*		
cover	NMR[mV]	Δt[s]	cover	NMR[mV]	Δt[s]
on	2.37	0	on	9.15	0
off	2.34	11	off	9.20	12
off	2.16	40	on	8.93	25
Depolarization rate [μV/sec.]					
6.2			8.8		
Effect on signal height [%]					
1.7			1.7		

Table 4.4: Results of tests for C_{cover}.

4.2.4 Cell Position and Flux

The amount of voltage produced in the pickup coils depends on four factors: the rate of spin precession (ω_o), the density of spins, the polarization, and the position of the target cell (Figure 4.4). The geometrical flux, Φ, is the number of magnetic field lines that pass through the pickup coils when the spins are on resonance. The contribution to Φ was calculated for each chamber using

$$\Phi = \oint_C \int_V \frac{\vec{m} \wedge \vec{r}}{\vec{r}^3} \vec{d}l dV. \tag{4.25}$$

Here, $\vec{m}$ is the density of magnetization for the target. It will be considered unit-less and therefore Φ will have the units of cm^2. The volume of a chamber is given by V, and the coil boundary is C. The target cell pumping chamber contribution to the flux was weighted by $\frac{(n_p/n_o)}{(n_c/n_o)}$ to reflect the fact that the density is not uniform. The total flux for each water signal was determined (Table 4.5), and studies of the dependence of the flux on cell position were done using Eq. 4.25.

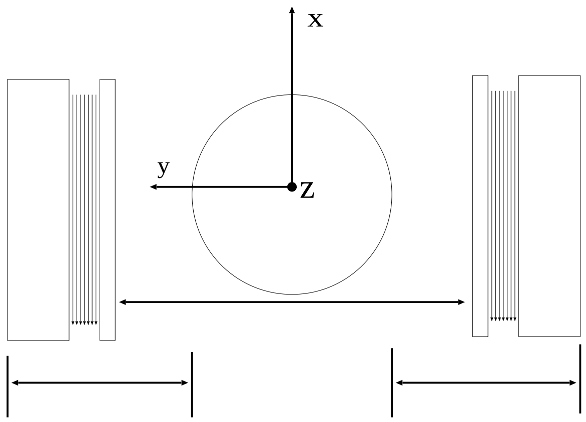

Figure 4.4: Positioning of the target chamber between the pickup coils.

The uncertainty in the amount of geometrical flux associated with each cell comes from two primary sources: the position of the cell in the y-direction and inner radius of the target chamber. Each time a cell was mounted, its position relative to the pickup coils was measured using a caliper. The uncertainty from this type of measurement is about ± 1.5 mm. This contributes an uncertainty of 1.0% to the total flux. The contributions from the uncertainty in the pickup coils in the x and z-directions, along with tilting and rotations, are all less than $\pm 0.3\%$. The inner radius of the target chamber is known to ± 0.05 mm. This leads to an uncertainty in the flux of $\pm 1.7\%$. The total uncertainty in the flux is assigned to be $\pm 2.1\%$ for all

Calibration date or Helium cell	Flux of each part (cm)			$\Phi_{He,w}$
	Target	**Pump**	**Transfer**	**Total**
9/25/98	46.33	-3.90	0.04	42.47
11/3/98	49.60	-3.92	-0.06	45.61
11/25/98	49.78	-3.92	-0.08	45.79
Don't Worry	44.31	-2.57	0.11	41.85
Be Happy	45.87	-3.28	0.10	42.69
Armageddon	44.32	-2.36	0.06	42.02
Nepheli	47.91	-2.50	0.01	45.42
Sysiphos	49.23	-2.58	0.04	46.69
Jin	47.71	-2.43	0.02	45.30

Table 4.5: The flux, Φ, for each water calibration and for each ^{3}He cell.

cells except *Armageddon*. The position of *Armageddon* was not recorded. Therefore, its flux uncertainty is derived from assuming that the cell could be anywhere along the y-direction and is set at $\pm 3.4\%$.

4.2.5 Coil Gain

One consequence of having target cells filled to 10 atmospheres is that they can explode. When this happens the explosions cause small changes in the gain of the LRC circuit. In order to monitor this effect, a small excitation coil was fixed within the RF Helmholtz coils. A RF signal was sent to the excitation coil which created a response in the pickup coils. By changing the frequency of the excitation coil, the pickup coils' Q-curve, or response curve, could be mapped out. The voltage induced in the pickup coils as a function of frequency, f, is given by:

$$V(f) = \frac{Af}{\sqrt{\frac{1}{Q^2}\frac{f^2}{f_0^2} + \left(\frac{f^2}{f_0^2} - 1\right)^2}}. \tag{4.26}$$

The numerator, Af, is the induced EMF. 'A' depends on geometric factors and the amplitude of the signal that drives the excitation loop. The parameters A,

f_0, and Q are determined by fitting the data to equation 4.26. G^Q is defined by $V(f = 91kHz)/(A \cdot 91kHz)$. The results of the calculated gain agree closely with one another (Figure 4.5).

It appears (Figure 4.5) that following *Armageddon* and *Nepheli*'s explosions there was a change in the Q-curve. The values of G^Q for the water signals taken on 9/25/98, 11/3/98, and 11/25/98 are 1.265, 1.260, and 1.255 respectively. For the target cells, G^Q is 1.265 for *Don't Worry*, *Be Happy*, and *Armageddon*, 1.260 for *Nepheli*, and 1.255 for *Sysiphos* and *Jin*.

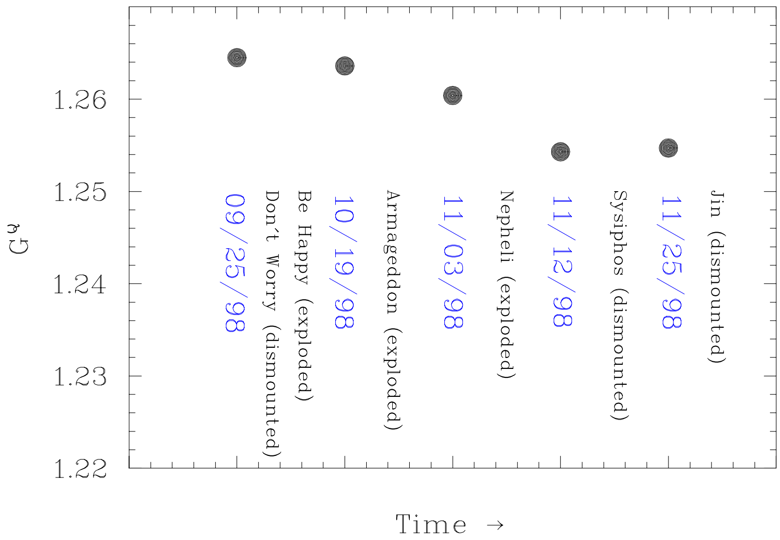

Figure 4.5: The value of G^Q as a function of time.

4.2.6 Calculation of κ_w^*

Recall that the water calibration constant κ_w^* is given by Eq. 4.12:

$$\kappa_w^* = \frac{S_w}{P_w^{th}} \cdot \frac{\mu_{He}}{\mu_p} \cdot \frac{G_{He}^{pre}}{G_w^{pre}} \cdot \frac{1}{G_w^Q} \cdot \frac{1}{\Phi_w} \cdot \frac{1}{n_p} \cdot C_{\frac{\delta H}{H}} \cdot C_{cover}.$$

The three water signal's *UP* and *DOWN* sweeps yield six measurements of κ_w^*. By combining the *UP* and *DOWN* S_w/P_w^{th} ratios, there will be only one κ_w^* for each water signal. These three κ_w^* are then averaged. Table 4.6 lists the input values for Eq. 4.12 and Figure 4.6 shows the results.

Parameter	Value	Uncertainty (%)
(S_w^{up}, S_w^{down})	(13.1,15.5), (6.48,7.83), (66.9,79.5) μV	1.3
P_w^{th}	6.415, 7.655 ($\times 10^{-9}$)	1.3
μ_{He}/μ_p	0.762	-
n_p	2482 amg.	0.1
G_{He}^{pre}/G_w^{pre}	1/200, 1/100, 1/1000	0.5
G_w^Q	1.2645, 1.2604, 1.2547	-
Φ_w	43.0, 46.2, 46.4 cm^2	2.1
$C_{\frac{\delta H}{H}}$	1.0035, 1.0156, 1.0099	0.2
C_{cover}	0.983	0.3
Total:κ_w^*	5.56×10^{-4} $\left[\frac{mV}{\%\cdot amg.\cdot cm^2\cdot Q-gain}\right]$	2.3

Table 4.6: The values for the parameters that go into calculating κ_w^* and their uncertainties.

The uncertainty on each point in Figure 4.6 is derived from those listed in Table 4.6. An estimate of the total systematic uncertainty on κ_w^* was calculated by considering the correlated and uncorrelated portions seperately:

$$\sigma_{(\kappa_w^*)} = \sqrt{\frac{1}{3}(\sigma^2_{(S_w)} + \sigma^2_{(P_w^{th})} + \sigma^2_{(G^{pre})} + \sigma^2_{(\Phi_w^{pos})} + \sigma^2_{(C_{\frac{\delta H}{H}})}) + \sigma^2_{(n_p)} + \sigma^2_{(\Phi_w^{rad})} + \sigma^2_{(C_{cover})}}. \tag{4.27}$$

The flux uncertainty was broken up into two parts: the uncorrelated uncertainty due to the position (1.2%) and the correlated uncertainty due to the inner radius (1.7%). The total uncertainty on the average of the three water signals is estimated to be ±2.3%. This uncertainty is similar to the one determined for the SLAC E154 experiment [50]. The value for κ_w^* is

$$\kappa_w^* = 5.56 \times 10^{-4} \left[\frac{\text{mV}}{\%\ \text{amg cm}^2\ \text{Q}}\right]. \tag{4.28}$$

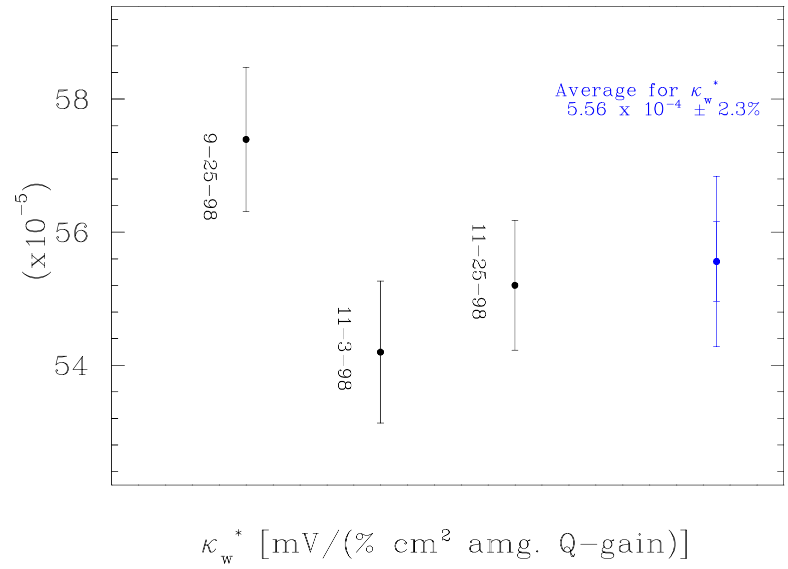

Figure 4.6: The value of κ_w^* for the three water signals.

4.2.7 The Calibration Constant κ_{epr}^*

The second method by which the NMR system was calibrated was to measure the separation of the ^{85}Rb $(F = 3, m = -3)$ and $(F = 3, m = -2)$ energy levels (Figure 3.1), or electron paramagnetic resonance (EPR). This separation, $\Delta\nu$, is proportional to the ^{3}He polarization in the pumping chamber: P_{He}^{pump}. The pumping chamber polarization is in turn related to the polarization measured by the NMR system: P_{He}^{targ}. Just as in the case of water, a NMR signal related to a known polarization allows for the calculation of κ^* as presented in Eq. 4.10. Explicitly, κ_{epr}^* is given as

$$\kappa_{epr}^* = \frac{S'_{He}}{P_{He}^{targ}} \cdot \frac{1}{G'^{Q}_{He} \cdot \Phi'_{He} \cdot n'_o \left(\frac{n'_c}{n'_o}\right)}. \tag{4.29}$$

Here, the prime indicates the quantities for the particular cell used during the calibration and P_{He}^{pump} is related to the EPR measurement.

There are three factors that account for the separation in energy levels: the holding field, the magnetic field caused by polarized ^{3}He, and the spin exchange of Rb-^{3}He.

The amount of separation caused by the magnetic field of the ^{3}He is proportional to its magnetization, M_{He} : $B_{He} = \frac{8\pi}{3} M_{He}$. The separation created by this field is small in comparison to the separation created by the holding field (≈11 GHz for 25 Gauss). Therefore, the ^{3}He magnetic field shift can be related to the derivative of the EPR frequency, $\nu(F, m)$, of the $(F, m \rightarrow F, m-1)$ transition:

$$\Delta\nu_M = \frac{d\nu(F,m)}{dB}\frac{8\pi}{3}M_{He} = \frac{d\nu(F,m)}{dB}\frac{8\pi}{3}[He]\mu_{He}P_{He}, \tag{4.30}$$

where $[He]$ is the ^{3}He number density, μ_{He} is the ^{3}He magnetic moment, and P_{He} is the amount of ^{3}He polarization. The spin exchange of Rb-^{3}He also creates a separation that is equivalent to an additional magnetic field:

$$B_{SE} = \frac{2\hbar K_{SE}\Gamma_{SE}}{g_e\mu_B}K_z, \tag{4.31}$$

where K_{SE} is the ratio of the imaginary and real parts of the spin-exchange cross section, $< v\sigma_{SE} >$ is the velocity averaged real part of the cross section, $g = 2$ for the electron, μ_B is the Bohr magneton, and K is the ^{3}He nuclear spin. Again, the separation created by B_{SE} is related to the derivative: $\Delta\nu = \frac{d\nu(F,m)}{dB}B_{SE}$.

The total separation of the $(F = 3, m = -3)$ and $(F = 3, m = -2)$ sublevels due to the polarized ^{3}He is

$$\Delta\nu = \Delta\nu_{SE} + \Delta\nu_M = \frac{8\pi}{3}\frac{d\nu(F,m)}{dB}\kappa_o\mu_{He}[He]P_{He}, \tag{4.32}$$

where κ_o is related to the spin-exchange cross section and does not depend on the ^{3}He density or polarization. It is normalized such that if only the magnetic field created by the polarized ^{3}He were considered, κ_o would equal one. However, $\kappa_o \approx 6$, which implies that there is an attraction between the Rb electron wavefunction and the ^{3}He

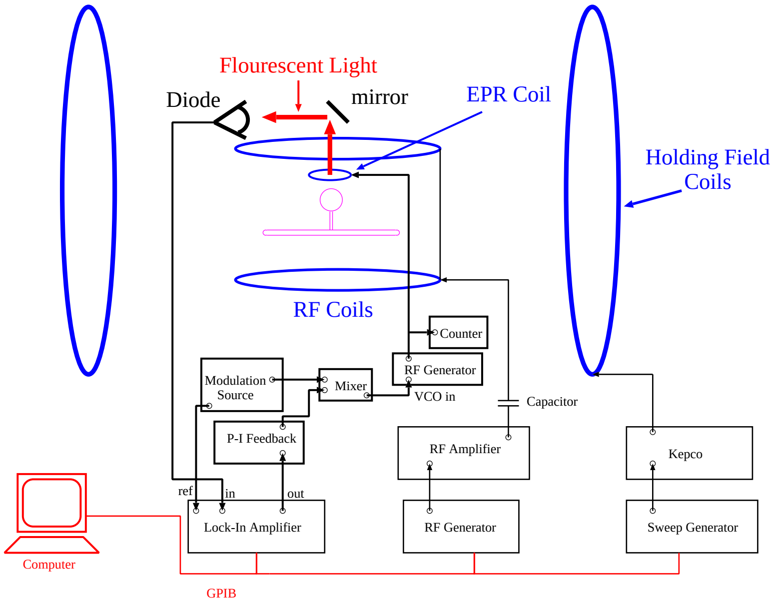

Figure 4.7: A schematic of the EPR electrons setup.

nucleus. The constant κ_o was measured explicitly by [65] and is known to $\pm 1.5\%$:

$$\kappa_o = 4.52 + 0.00934 \cdot T(^\circ\mathrm{C}). \tag{4.33}$$

The derivative of the EPR frequency $\left(\frac{d\nu(F,m)}{dB}\right)$ for the $(F = 3, m = -3 \rightarrow F = 3, m = -2)$ transition is given by the Breit-Rabi equation [68]:

$$\frac{dv(F,m)}{dB} = \frac{\mu_B g_e}{h(2I+1)}\left(1 + \frac{8I}{(2I+1)^2}\frac{\mu_B g_e B}{hA}\right), \tag{4.34}$$

where $I = 5/2$ and $A = 1012$ MHz for ^{85}Rb. Substituting Eq. 4.34 into Eq. 4.32, the ^{3}He polarization can be written as

$$P_{He}^{pump} = 0.852 \left[\frac{\text{amg.}}{\text{kHz}}\right] \frac{\Delta\nu}{\kappa_o n'_o \left(\frac{n'_p}{n'_o}\right)}. \tag{4.35}$$

4.2.8 EPR System

Measurement of the EPR shift, $\Delta\nu$, was performed by observing the D2 fluorescent light emitted by decaying rubidium. This fluorescent light was observed with a photodiode (Figure 4.7). The intensity of the fluorescence is inversely proportional to the amount of Rb polarization. This is because only atoms that are not polarized can be excited and then give off a photon. By inducing the transition of the rubidium's outer electron from the $(F = 3, m_F = -3)$ state (a non excitable state) to the $(F = 3, m_F = -2)$ state (an excitable state) with a small coil located above the pumping chamber (EPR coil), the amount of optical pumping will increase and therefore the amount of fluorescence. The frequency of the $m_F = -3 \rightarrow -2$ transition is proportional to the holding field plus the field created by the polarized ^{3}He.

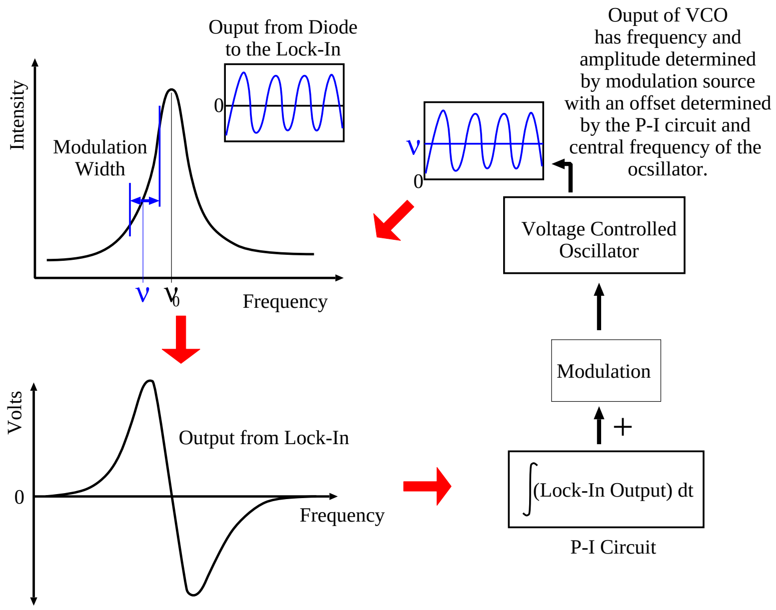

Figure 4.8: The feedback mechanism for the EPR setup.

It was necessary to lock onto the EPR resonance because of drifts in the holding field. This was done by using a feedback mechanism (Figure 4.8). The driving frequency for the EPR coil was modulated by 6 kHz at a frequency of 200 Hz. This in turn swept out a portion of the intensity spectrum which created a sine wave whose

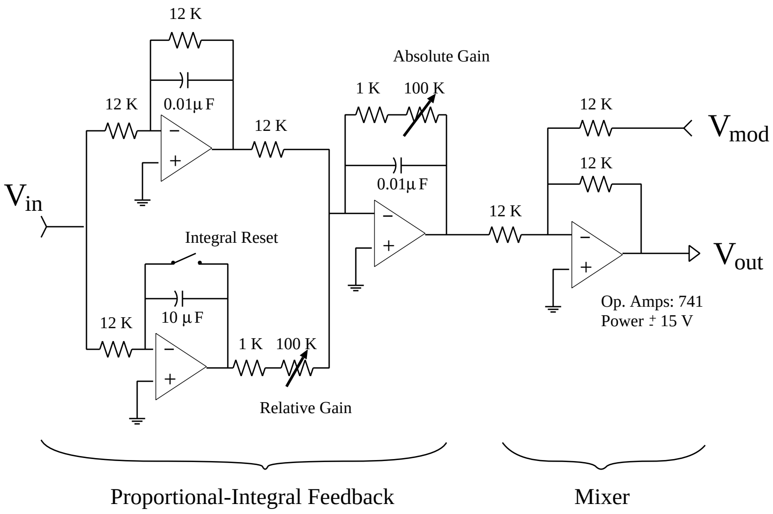

Figure 4.9: Circuit diagram for the proportional-integral feedback and the mixer.

amplitude depended on the value of the central driving signal (ν) in relation to the resonance frequency (ν_o). The output of diode was read by the lock-in amplifier. The lock-in output was proportional to the amplitude of the sine wave; it was zero on and far off resonance. The output of the lock-in was integrated and mixed with a modulation signal using a P-I/Mixer circuit (Figure 4.9). This signal was then sent into the *Wavetek Model 80* Voltage Controlled Oscillator (VCO) whose output was a sine wave with a central frequency determined by the value set on the device and the integral of the lock-in. This frequency was varied by the modulation source and was used to drive the EPR coil. As an example, assume that the frequency ν is less than ν_o. The lock-in detects a sine wave and outputs a positive signal which is then integrated. The positive signal from the P-I feedback box, along with the modulation signal, is inputed into the VCO and causes the signal to shift to a higher frequency. The frequency ν is now closer to ν_o. It was in this way that the feedback mechanism moved and kept the central frequency ν at the same value of the resonance frequency ν_o.

In order to isolate the shift contribution related to the polarized ^{3}He, a measurement was first done with the spins in one direction and then reversed (Figure 4.10).

The flip was performed using AFP, by changing the RF field to induce the transition.

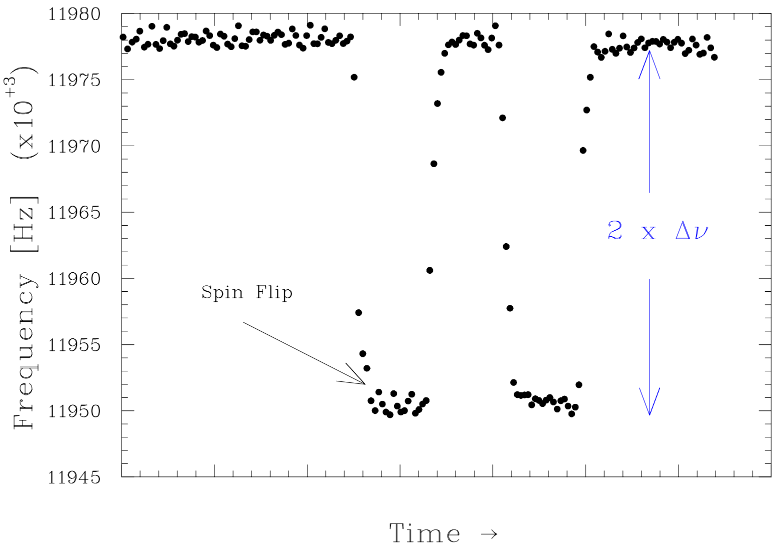

Figure 4.10: An EPR measurement showing the change in resonance frequency due to the ^{3}He spins being flipped.

4.2.9 Polarization Gradient

If the target cell (Figure 3.3) were comprised of only one chamber, then a direct comparison between the EPR shift and a NMR signal could be made. However, with a two chamber cell the ^{3}He polarization originates in the pumping (top) chamber and diffuses down into the target (bottom) chamber. In order to relate an EPR measurement to a NMR measurement, understanding of this transfer of polarization is necessary.

The flux of ^{3}He atoms, with desired spin direction, along the transfer tube is given by

$$\mathcal{J}(z) = \frac{1}{2} n(z) D(z) \frac{dP}{dz} = \text{constant}, \tag{4.36}$$

where $n(z)$ is the number density along the transfer tube, $D(z)$ is the diffusion coefficient, and P is the amount of polarization. The diffusion coefficient at 1 atm. and

80°C is 2.76 cm^2/s [69]. This is related to $D(z)$ by the following relation:

$$D(z) = 2.76[cm^2/s]\frac{0.773amg.}{n(z)}\left(\frac{T(z)}{353^\circ K}\right)^{m-1}, \tag{4.37}$$

where $m = 1.7$ [69]. The temperature distribution, $T(z)$, along the transfer tube is $T(z) = T_t + \frac{T_p - T_t}{L_{tran}}(z + \frac{L_{tran}}{2})$. By integrating Eq. 4.36 along the length of the transfer tube, the polarization flux can be expressed in terms of the pumping and target chamber polarizations:

$$\mathcal{J} = \frac{D_t n_t K}{2L_{tran}}(P^{pump} - P^{targ}). \tag{4.38}$$

Here, D_t is the diffusion coefficient at the target chamber and $K = \frac{(2-m)(T_p - T_t)T_t^{1-m}}{T_p^{2-m} - T_t^{2-m}}$.

Knowing the polarization flux, the time rate-of-change for each chamber is given by:

$$\frac{dP^{pump}}{dt} = -G_p(P^{pump} - P^{targ}) \qquad \text{and} \qquad \frac{dP^{targ}}{dt} = -G_t(P^{targ} - P^{pump}), \tag{4.39}$$

where

$$G_p = \frac{A_{tran} n_t}{V_p L_{tran} n_p} D_t K \qquad \text{and} \qquad G_t = \frac{A_{tran}}{V_p L_{tran}} D_t K. \tag{4.40}$$

However, even these equations are not enough to describe the polarization in each chamber, for they only describe the diffusion of the gas from one chamber to the next. For a complete description of the polarization the effects of spin exchange and depolarization need to be included. The complete rate equations for the polarization in terms of the cell lifetime, Γ, and the spin exchange rate, γ_{SE}, are

$$\frac{dP^{pump}}{dt} = -G_p(P^{pump} - P^{targ}) + \gamma_{SE} < P_{Rb} > -(\gamma_{SE} + \Gamma)P^{pump} \tag{4.41}$$

$$\frac{dP^{targ}}{dt} = -G_t(P^{targ} - P^{pump}) + \Gamma P^{targ}. \tag{4.42}$$

The solution to this set of coupled equations is

$$P^{pump,targ}(t) = A_1^{pump,targ} e^{-\gamma_{slow}t} + A_2^{pump,targ} e^{-\gamma_{fast}t} + P_\infty^{pump,targ}, \tag{4.43}$$

where $A_{1,2}$ are constants and $P_\infty^{pump,targ}$ are the saturation polarizations given by

$$P_\infty^{pump} = \frac{\gamma_{SE}}{G_p + \gamma_{SE} + \Gamma + \frac{G_p G_t}{\Gamma + G_t}} < P_{Rb} > \quad \text{and} \quad P_\infty^{targ} = \frac{G_t}{\Gamma + G_t} P_\infty^{pump}. \tag{4.44}$$

The term that goes like $e^{-\gamma_{fast}t}$ in Eq. 4.43 vanishes and can be neglected. Solving for $e^{-\gamma_{slow}t}$, a linear relation between the target and pumping chamber polarizations is formed:

$$P^{targ} = \alpha_1 P^{pump} + \alpha_2, \tag{4.45}$$

where

$$\alpha_1 = \frac{\gamma_{fast} P_\infty^{targ}}{\gamma_{fast} P_\infty^{pump} - \gamma_{SE} < P_{Rb} >}, \tag{4.46}$$

$$\alpha_2 = P_\infty^{targ} \left(1 - \frac{\gamma_{fast} P_\infty^{targ}}{\gamma_{fast} P_\infty^{pump} - \gamma_{SE} < P_{Rb} >}\right), \tag{4.47}$$

and

$$\gamma_{fast} = \frac{1}{2}\left[G_t + G_p + 2\Gamma + \gamma_{SE} + \sqrt{(G_t - G_p - \gamma_{SE})^2 + 4G_p G_t}\right]. \tag{4.48}$$

The polarization of the target chamber, P_{He}^{targ}, can now be calculated from the EPR shift using Eqs. 4.45 and 4.35. The difference in pumping and target chamber polarizations, ΔP, were typically $\sim$1% (Table 4.7).

4.2.10 Calculation of κ_{epr}^*

In order for Eq. 4.45 to be valid, the pumping system (e.g., number of lasers on, temperature, etc.) has to be stable. Nine EPR calibrations were done during the experiment using four different cells (Figure 4.11). Parameters for each calibration

#	Cell	$\Delta\nu$ [kHz]	$S'_{He}[mV]$	$\left(\frac{n'_c}{n'_o}\right)$	$\left(\frac{n'_p}{n'_o}\right)$	ΔP [%]	κ^*_{epr} [$\times 10^{-4}$]
1	*Don't Worry*	8.15	4.26	1.112	0.919	0.03	5.46
2	*Nepheli*	11.77	6.37	1.214	0.808	1.26	5.22
3	*Nepheli*	13.74	8.01	1.215	0.807	1.24	5.54
4	*Nepheli*	16.64	9.57	1.213	0.810	1.13	5.40
5	*Sysiphos*	14.02	8.80	1.209	0.808	1.03	5.70
6	*Jin*	16.70	10.10	1.159	0.826	0.50	5.89
7	*Jin*	17.11	11.76	1.223	0.786	0.87	6.19
8	*Jin*	18.03	11.64	1.209	0.801	0.77	5.95
9	*Jin*	13.24	8.08	1.166	0.818	0.97	6.08

Table 4.7: Conditions for the nine EPR calibrations. ΔP is the difference between the pumping and target chamber polarizations.

are listed in Table 4.7.

The calculation of two new parameters, $< P_{Rb} >$ and γ_{SE} (Eq. 4.41), were needed to complete the EPR calibration. The spin exchange rate for Rb-^{3}He, γ_{SE}, is given as a function of temperature by [57, 52]:

$$\gamma_{SE} = 6.7 \times 10^{-20} \left[\frac{\text{cm}^3}{\text{s}}\right] \cdot (1.507 \times 10^{26}) \frac{10^{-4040/T}}{T} [\text{cm}^{-3}], \tag{4.49}$$

where T is the lowest temperature inside the pumping chamber. Typically, the low temperature spot was near the bottom of the pumping chamber. A RTD was placed near that spot: rtd#7. So, T is taken to be the value read by rtd#7. The average Rb polarization, $< P_{Rb} >$, was estimated from the spin-up curves performed on various cells and applying Eq. 3.4. The results provided a range of values from 60 to 90%.

The value and uncertainty for κ^*_{epr} was calculated by taking a weighted average of the nine EPR measurements. Correlated and uncorrelated uncertainties were treated separately (Table 4.8). The χ^2_ν for the average of κ^*_{epr} for each cell was found to equal 3, this implies that the uncertainty for each cell is underestimated. To take this into account, each uncertainty was multiplied by a factor, $f = 1.725$, such that the χ^2_ν was equal to one. This same factor was then applied to the original error on the weighted

Parameter	Uncer. in Parameter	Uncer. in κ^*_{epr} [%]
Totally Uncorrelated		
$\Delta\nu$	± 50 Hz	0.4
$< P_{Rb} >$	± 0.15	2.0
T_p	$\pm 18°$C	1.4
T_c	$\pm 1.1\%$	1.2
rtd#7	$\pm 5°$C	2.0
Correlated by cell		
n_o	$\pm 1.2\%$	0.1
Φ'_{He}	$\pm 2.1\%$	2.1
Correlated between cells		
κ_o	$\pm 1.5\%$	1.5

Table 4.8: Uncertainties contributing towards the total uncertainty on κ^*_{epr}.

mean. The final estimated uncertainty for κ^*_{epr} is $\pm 2.8\%$, where

$$\kappa^*_{epr} = 5.66 \times 10^{-4} \left[\frac{\text{mV}}{\%\ \text{amg. cm}^2\ \text{Q}}\right]. \tag{4.50}$$

4.3 Elastic Peak Asymmetry

The constant κ^* as determined using water and EPR was checked by measuring the asymmetry in elastic scattering for electrons by a polarized ^{3}He target (Section 1.2). Two sets of elastic data were taken: at $E = 0.862$ GeV and $E = 1.72$ GeV. With this data a raw asymmetry is formed:

$$A^{Raw}_{elas} = \frac{N^{\uparrow\uparrow} - N^{\uparrow\downarrow}}{N^{\uparrow\uparrow} + N^{\uparrow\downarrow}}, \tag{4.51}$$

where $\uparrow\uparrow$ ($\uparrow\downarrow$) refers to the case when the electron and target spins are parallel (anti-parallel) with one another. N is the counting rate of elastically scattered electrons normalized to the beam current.

The raw asymmetry is related to the asymmetry (Eq. 1.17) associated with elastic

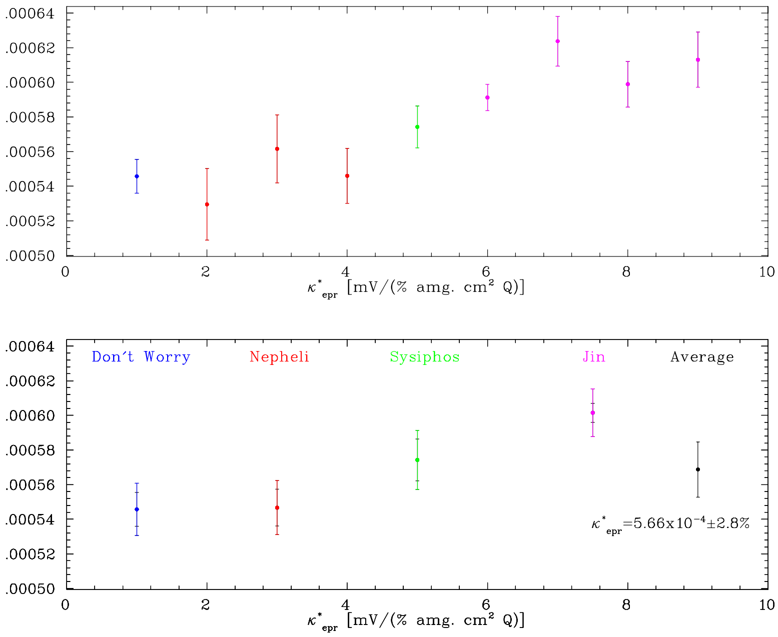

Figure 4.11: The nine EPR measurements for κ^*_{epr}. Multiple measurements for one cell were averaged before a total average of all four cells was determined.

electron scattering by

$$A^{phys}_{elas} = \frac{A^{Raw}_{elas}}{f \cdot P_b \cdot P_t}, \tag{4.52}$$

where P_b is the polarization of the electron beam, P_t is the polarization of the target, and f is the dilution factor. The dilution factor is simply the fraction of scattered electrons considered to be produced from an elastic collision compared to the total. Mistaken events mostly come from the scattering of the electrons by N_2 gas in the target cell. The dilution factor is approximately 0.993 for the 0.862 GeV data and 0.915 for the 1.72 GeV data.

A Monte Carlo simulation, that corrects for the spectrometer's acceptance and the target's spatial dimensions, was used to generate an expected asymmetry: $A^{M.C.}$. By comparing this asymmetry to the raw asymmetry, a κ^*_{elas} was calculated using

$$\kappa^*_{elas} = \frac{S_{He}}{\frac{A^{Raw}}{A^{M.C.} f P_b} \Phi_{He} G^Q n_o \left(\frac{n_c}{n_o}\right)}. \tag{4.53}$$

Systematic Uncertainties [%]	
P_b	3.0
$A^{M.C.}$	3.0
n_o	1.0
Φ_{He}	2.1
(n_c/n_o)	2.0
Total	5.2
Statistical Uncertainties [%]	
A^{Raw}(0.862 GeV)	3.5
A^{Raw}(1.72 GeV)	10

Table 4.9: Systematic and statistical uncertainty on κ^*_{elas}.

The results for the two energies are

$$\kappa^*_{elas}(0.862\text{GeV}) = 6.10 \times 10^{-4} \quad \text{and} \quad \kappa^*_{elas}(1.72\text{GeV}) = 5.99 \times 10^{-4}. \qquad (4.54)$$

The uncertainties for these values are listed in Table 4.9 [70].

4.4 Calibration Results

Results for κ^* show good agreement between κ^*_{epr}, κ^*_w, and κ^*_{elas} (Figure 4.12). The final result for κ^* was calculated by taking the weighted average of κ^*_{epr} and κ^*_w. It has an uncertainty of $\pm 1.8\%$:

$$\kappa^* = (5.60 \pm 0.10) \times 10^{-4} \left[\frac{mV}{\% \cdot \text{amg.} \cdot \text{cm}^2 \cdot Q^2} \right]. \qquad (4.55)$$

To calculate the constant of proportionality that relates the NMR signal to polarization, recall Eq. 4.10:

$$\kappa_{cell} = \kappa^* \Phi_{He} G^Q n_o \left(\frac{n_c}{n_o} \right).$$

Each of the parameters in Eq. 4.10 has been calculated and their uncertainties es-

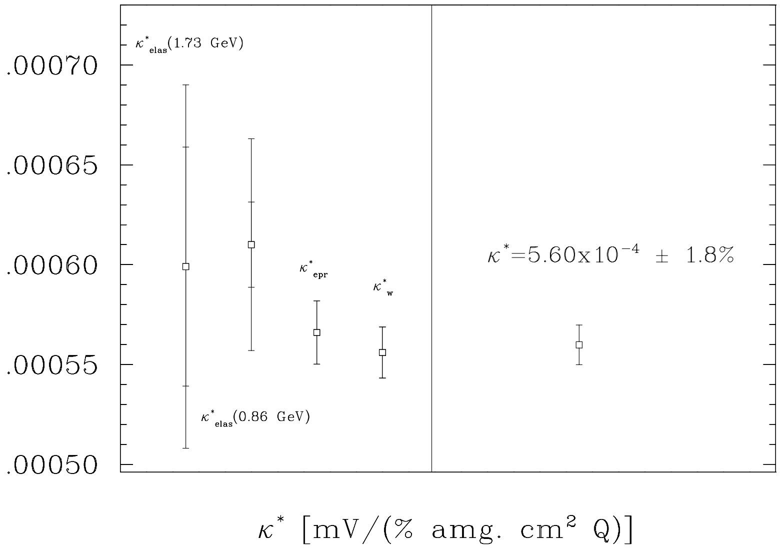

Figure 4.12: Results of the four NMR system's responsiveness, κ^*, measurements.

timated (Table 4.10). The total uncertainty assigned to κ is $\pm 3.6\%$ ($\pm 4.5\%$ for *Armageddon*). The values, depending on which cell was in use, that were used to calculate the polarization of the target are listed in Table 4.11.

Parameter	Value	Uncertainty (%)
κ^*	5.60×10^{-4}	1.8
Φ_{He}	Table 4.5	2.1
G^Q	Section 4.2.5	-
n_o	Table 3.5	1.0
$\left(\frac{n_c}{n_o}\right)$	Table 3.6	2.0
Total		3.6

Table 4.10: Contributions towards the total uncertainty on κ.

4.5 Target Performance

NMR measurements of the target's polarization were taken approximately every four hours throughout the experiment. Each data "run" lasted about 20-30 minutes and

$\kappa_{Don'tWorry}$	$\kappa_{BeHappy}$	$\kappa_{Armageddon}$	$\kappa_{Nepheli}$	$\kappa_{Sysiphos}$	κ_{Jin}
0.355	0.343	0.354	0.432	0.320	0.317

Table 4.11: Values of κ for each cell in units of [mV/%].

was assigned an NMR value based upon a linear interpolation of NMR signals taken before and after the run. Depending on the cell used, the signal was divided by κ to give the polarization for that run. Results on the polarization measurements are shown in Figure 4.13. The average polarization for the experiment was $\sim$33%.

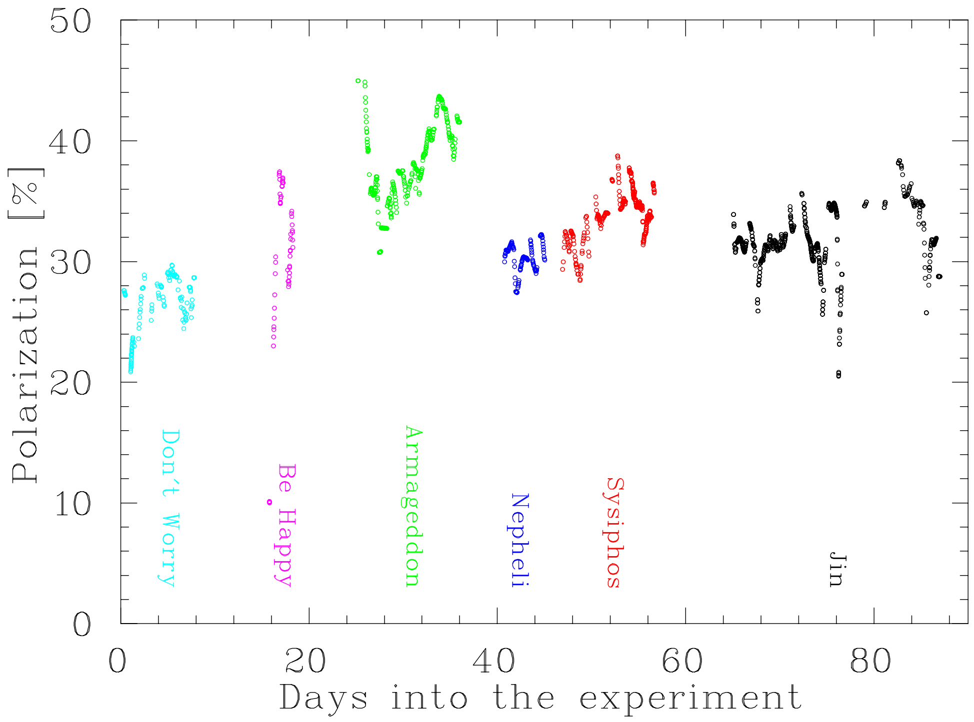

Figure 4.13: The polarization as a function of time for all of the data taken during experiment E94-010.